Arch. Metall. Mater. **64** (2019), 3, 969-974

DOI: 10.24425/amm.2019.129482

S. KĄC*#, G. SZWACHTA*, Ł. CIENIEK*, T. MOSKALEWICZ*

MORPHOLOGY AND STRUCTURE OF THE ERBIUM STABILIZED BISMUTH OXIDE THIN FILMS DEPOSITED BY PLD TECHNIQUE

The aim of the work was to obtain thin bismuth oxide films containing, at room temperature, the $Bi_{1,5}Er_{0,5}O_3$ phase. This phase corresponds to the structure of the high-temperature δ-Bi_2O_3 phase, in pure bismuth oxide, characterized by the highest ionic conductivity of all known solid state ionic conductors. The high-temperature δ-Bi_2O_3 phase with the face centered cubic structure, in pure bismuth oxide, occurs only at temperature above 730°C.

Stabilization of the δ-Bi_2O_3 phase at room temperature was achieved by an addition of the erbium together with the employment of the Pulsed Laser Deposition (PLD) technique. The influence of an amount of Er alloying and the film thickness on surface morphology, microstructure, phase composition of thin films were investigated. The velocity of deposition of thin layers of bismuth stabilized with erbium in the PLD process using the Nd: YAG laser was about 0.5 nm/s.

The investigation results of erbium doped bismuth oxide thin films deposited onto (0001) oriented Al_2O_3 monocrystalline substrate are presented.

Thin films of uniform thickness, without cracks, and porosity were obtained. All deposited thin films (regardless of the film thickness or erbia (Er_2O_3) content) exhibited a columnar structure. In films stabilized with erbium, up to approx. 250 nm thickness, the columns have a diameter at the base from 25 to 75 nm. The columns densely and tightly fill the entire volume of the films. With increasing of the film thickness increases, porosity also significantly increases. In thin layers containing from 20 to 30 mole % Er_2O_3 the main identified phase at room temperature is $Bi_{1.5}Er_{0.5}O_3$. It is similar to the defective fluorite-type structure, and belongs to the Fm-3m space group. This phase corresponds to the structure of the high-temperature δ-Bi_2O_3 phase in pure bismuth oxide.

Keywords: Pulsed Laser Deposition, thin films, bismuth oxide, surface topography

1. Introduction

Bismuth oxide, both pure and doped, although discovered over one hundred years ago, is still considered as one of the most promising material in Nanoionics and Iontronics disciplines. This is evidenced by articles published in recent years in high quality scientific journals [1-6]. The practical use of this material is considered, among others, in the strategic field of science and technology, in the energy sector, for example, as an element of fuel cells (electrolyte in μ-SOFC – micro Solid Oxide Fuel Cells), elements of lithium-ion batteries (battery anodes), as well as elements such as gas sensors or materials for biosensors. So far, these materials have been tested for potential applications as sensors, catalysts, dyes, superconductors, scintillators, photocatalysts, high-temperature solid electrolytes and materials used to record information, photovoltaic cells and microwave integrated circuits [7]. Bismuth oxide is also widely used in optoelectronics for optical layers as well as for the production of superconducting ceramic glasses [8]. Some technological applications of this material in the form of thin layers depend on their surface condition which affects their photocatalytic properties and the ability to capture polarized gases in gas sensors [9-14]. This oxide exhibits a characteristic polymorphism. It may occur in polymorphic forms [10,11], however, the high temperature δ phase is among the most efficient oxide conductors. Unfortunately the δ phase is stable only above 730°C, up to a melting point of 824°C [7,9,14].

Numerous literature studies show that it is possible to stabilize the high temperature δ phase to lower temperatures, even to room temperature, by doping it with the various metal cations [10,15-18]. However this is often related to a significant decrease in the ionic conductivity, compared to the conductivity of pure δ phase [10,19]. The high temperature phase can be stabilized to a lower temperatures by different methods and techniques: layer formation [20,21], ion spraying in the high frequency field [14], pyrolysis [22], oxidation of thin bismuth layers [10,23], bismuth evaporation in oxygen atmosphere [10], electroplating [24], PVD (physical vapour deposition) methods [25], sol-gel method [10], CVD (chemical vapour deposition) [25] and MBE (molecular beam epitaxy) [26]. However, many of these techniques, are expensive and often quite complicated in technology. In addition, some materials and reagents used for these methods leave carbon

* AGH UNIVERSITY OF SCIENCE AND TECHNOLOGY, FACULTY OF METALS ENGINEERING AND INDUSTRIAL COMPUTER SCIENCE, AL. MICKIEWICZA 30, 30-059 KRAKOW, POLAND

Corresponding author: slawomir.kac@agh.edu.pl

impurities in the oxide layers. The preferred ones, because less expensive and less complicated that allow for the formation of oxide layers (e.g. Bi_2O_3) are, for example, the sol-gel method [9] and, for the sake of material purity, pulsed laser deposition (PLD) [16,17,27-33].

Additionally, isovalent and aliovalent substitution of Bi^{3+} by other cations can lead to stabilization of fluorite type structures to room temperatures [33-35]. The erbium atoms present in the bismuth oxide lattice provide the highest conductivity among all single rare-earth dopant systems.

Most of the papers regarding erbia stabilized bismuth oxide (ESB) refer to bulk materials prepared by powder technology. Only a few of them focused on the on the preparation and characterization of thin films [15,16]. The aim of this research was to comprehend the influence of PLD process parameters on the structure of ESB. Moreover, the change of dopant concentration was concerned as the reason of evolution of morphology and microstructure of as-deposited thin films.

2. Experimental

Erbia stabilized bismuth oxide films were deposited using pulsed laser deposition technique onto the single-crystal c-plane sapphire (0001), using a λ = 266 nm Nd:YAG laser system (Continuum Electro-Optics Inc.) with energy density (ρ) of ~3 J/cm^2, with a laser pulse width of 12 ns, and applied repetition rate of pulses of 10 Hz. A high-vacuum chamber was initially evacuated to 5×10^{-7} Torr using a combination of mechanical and turbo molecular pumps. Thin films were then deposited at the oxygen pressure of 100 mTorr. The sapphire substrates were ultrasonically cleaned with acetone, ethanol, and deionized water for 10 min. The substrates were placed in front of the target surface at the distance of 8 cm. The substrate temperature was 600°C. In order to analyze the influence of thin film thickness on their morphology, thin films of different thickness were produced: thinner, about 150-250 nm and thicker, 1.2-2.2 mm thick.

The synthesis of the powder with composition of (1 – x) Bi_2O_3–xEr_2O_3 (x = 0.20, 0.25, 0.30) was performed using mechanical alloying technique. The stoichiometric mixture of dried oxide powders (Sigma-Aldrich, Bi_2O_3 99.9% purity and Sigma-Aldrich, Er_2O_3 99.9% purity) after mixing were compacted by pressing into tablets and sintered at 800°C in air for 12 hours. The details of PLD processing have been reported in our previous paper [33].

The microstructure of thin films was investigated by scanning electron microscopy (FEI Nova NanoSEM) and transmission electron microscopy (TEM, JEOL JEM-2010ARP). The lamellas for TEM investigations were excised using a focused-ion beam device (FIB, FEI Quanta 3D 200i). Phase identification was performed by means of selected area electron diffraction (SAED) and supplemented by energy dispersive X-ray spectroscopy (STEM-EDS). The diffraction patterns were interpreted with the help of JEMS software.

The phase composition of deposited thin films was investigated by means of X-ray diffractometry (XRD), applying Panalytical Empyrean DY 1061 device with CuKα radiation (1.54 Å). The morphology and the surface topography were studied by atomic force microscopy (AFM, Veeco Dimension® Icon™ SPM) using a tapping mode.

3. Results and discussion

The thin film surface was smooth, with nanostructure. Only a few droplets were visible on the surface. The SEM images of the ESB thin films surface are presented in the figures 1 and 2.

All bismuth oxide thin films, regardless of the amount of Er dopant, have a columnar structure (Fig. 3, 4). However, depending on the film thickness, the columns have different sizes and shape that vary degrees of filling and compaction. In the case of films having low thickness, in the range of 150-250 nm), the material is compact. The columns densely and tightly fill the entire volume of the films (Fig. 1, 3). It is visible both on SEM

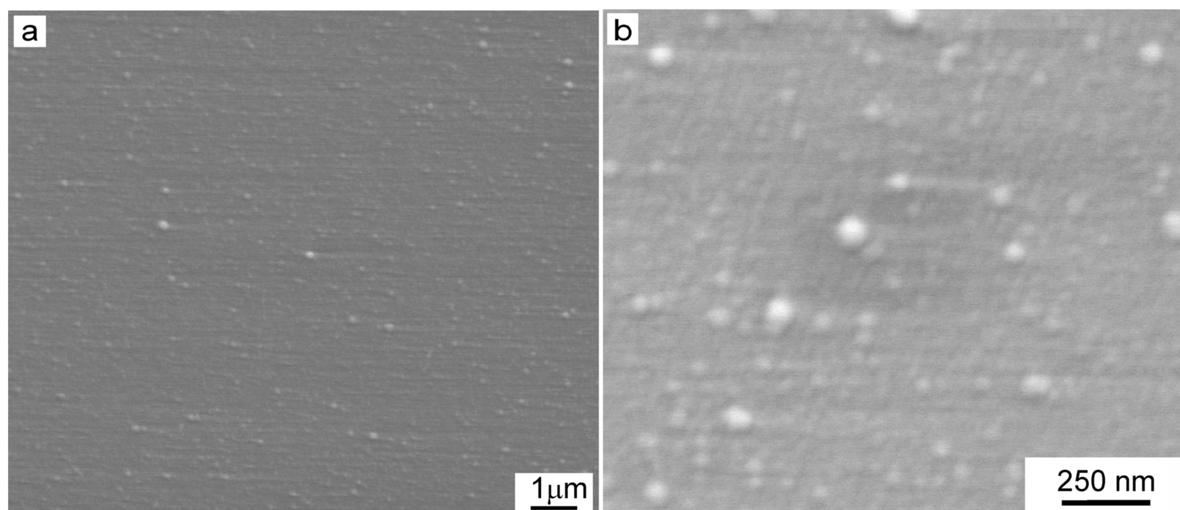

Fig. 1. SEM images of the $Bi_{1.5}Er_{0.5}O_3$ (Bi_2O_3 + 25 % mol. Er_2O_3) (a); magnified part of the image 1(a); λ = 266 nm, ρ = 3,0 J/cm^2, T_s = 600°C (b), film thickness 150 nm

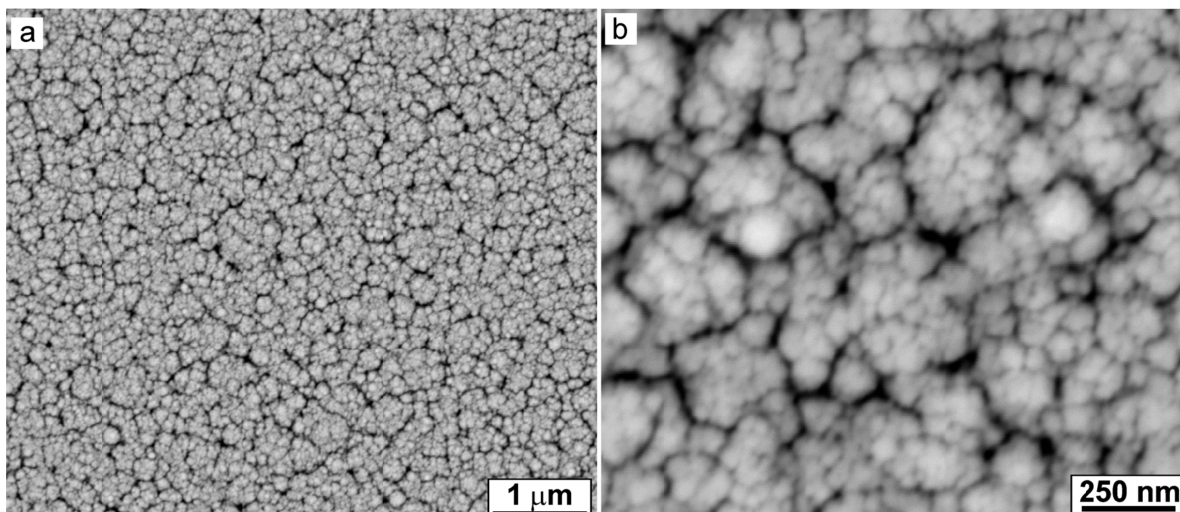

Fig. 2. SEM image of the $Bi_{1.5}Er_{0.5}O_3$ (Bi_2O_3 + 25 % mol. Er_2O_3) (a); (b), magnified part of the image 2(a); λ = 266 nm, ρ = 3,0 J/cm^2, T_s = 600°C, film thickness 2.5 μm

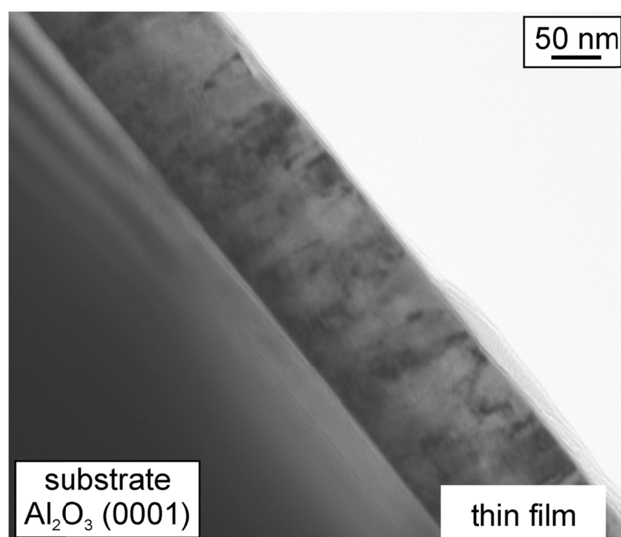

Fig. 3. TEM microstructure of fcc $Bi_{1.5}Er_{0.5}O_3$ (Bi_2O_3 + 25 % mol. Er_2O_3); film thickness 150 nm

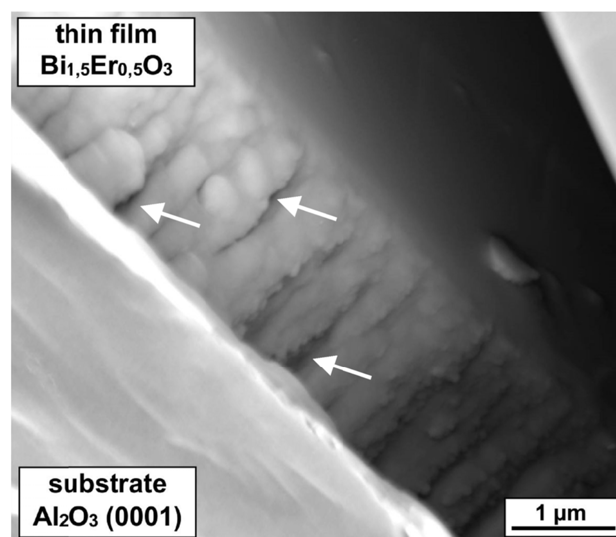

Fig. 4. Cross-sectional SEM image of fcc $Bi_{1.5}Er_{0.5}O_3$ (Bi_2O_3 + 25 % mol. Er_2O_3) thin film; film thickness 2.5 μm

images on the surface of thin layers and on their cross-sections in TEM images. The diameters of the columns range from 25 to 75 nm. In the case of thick films (in the range of 1.5-2.5 mm) the columns have a diameter of 100-160 nm. However, they are not so compact, there are empty spaces between the columns (Fig. 2, 4).

In the PLD process it is possible to deposit thin films by stoichiometric transfer of the target material to the substrate. Therefore, first in the mechanical alloying process, targets were prepared, in which the main phase was $Bi_{1.5}Er_{0.5}O_3$. This face-centered cubic phase has been described in solutions containing 17.5-45.5 mol % of erbia [36,37]. Below and above this range, the solid solutions were essentially multiphase.

The XRD phase analysis (Fig. 5) confirmed the occurrence of this phase in targets containing 20, 25 and 30 mole % of Er_2O_3. On the diffraction patterns, it can be seen that as the content of erbium increases, peaks from particular planes – especially for planes with higher indices – are shifted to the right, i.e. to the direction of higher values of the 2Θ angle. This is due to the fact that erbium ions have a smaller radius (1.030 Å for Er and 1.17 Å for Bi) [34,38]. The introduction of an addition of erbium into bismuth oxide results in the reduction in the lattice parameter of the obtained phase. Therefore, with the increase of erbium content, the lattice parameter is getting smaller and thus the larger peak shift towards higher values of the 2Θ angle.

As shown in figure 6, the main phase, identified in thin films deposited using targets containing 20, 25, 30 mol. % of Er_2O_3, is $Bi_{1.5}Er_{0.5}O_3$. It is the same phase which was identified in the targets (Fig. 5). For the films containing 20 and 30 mol. % of Er_2O_3 the preferred orientation texture of the (111) phase is visible while for 25 mol. % of erbia the (311) is preferential. However, this texture is not as strong as the texture observed in the niobium doped bismuth oxides films that was reported in our previous paper [33]. This preferred film orientation is due to deposition of thin films on Al_2O_3 single-crystal substrate with the

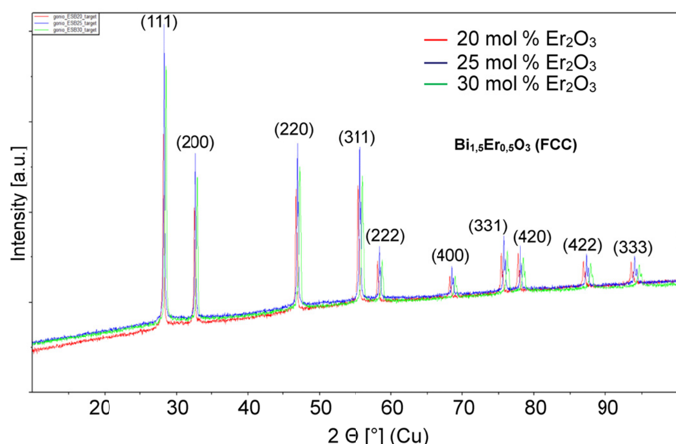

Fig. 5. X-ray diffraction patterns for $Bi_{1.5}Er_{0.5}O_3$ targets

orientation (0001). However, the results of investigations dealing with Y-stabilized Bi_2O_3 films [39] showed nearly identical levels of ionic conductivity in both the epitaxial and polycrystalline films, indicating that the extremely high grain boundary densities do not significantly affect the oxygen-ion conduction. Those observations suggest that Er stabilized Bi_2O_3 can be powerful thin-film electrolyte capable of producing high-performance outcomes without any deleterious effects, even when used with nanoscale thin films having extremely high density levels of the grain boundaries.

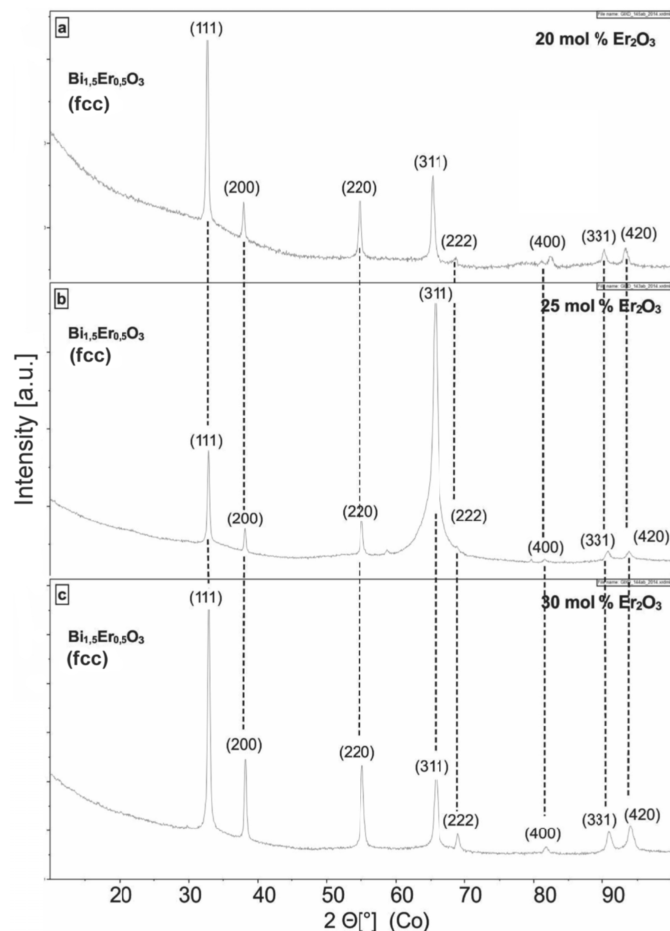

Fig. 6. X-ray diffraction patterns for $Bi_{1.5}Er_{0.5}O_3$ thin films deposited onto the sapphire substrate at T_{sub} of 600°C; (a) 20 mol % Er_2O_3, (b) 25 mol % Er_2O_3, (c) 30 mol % Er_2O_3

TEM images of erbium stabilized bismuth oxide thin films (Fig. 3) show their uniform thickness, which, in this case, depends mainly on the time of deposition. It is known that the film thickness is affected also by the energy density of the laser beam, the beam wavelength and the gas pressure in the reaction chamber.

In order to obtain thin films which are uniform, in respect of thickness, free of droplets or sputtered target particles, during the optimization of the PLD process, the parameters were selected so that the thickness of the deposited layers was mainly dependent on the duration of the process. In applied PLD process using the Nd:YAG laser, the deposition velocity of the erbium stabilized bismuth thin films of was therefore about 0.05 nm/laser pulse, i.e. about 0.5 nm/s. TEM investigations showed that thin films, stabilized with erbium, were characterized by a columnar structure (Fig. 7a, b). For films with the thickness of about

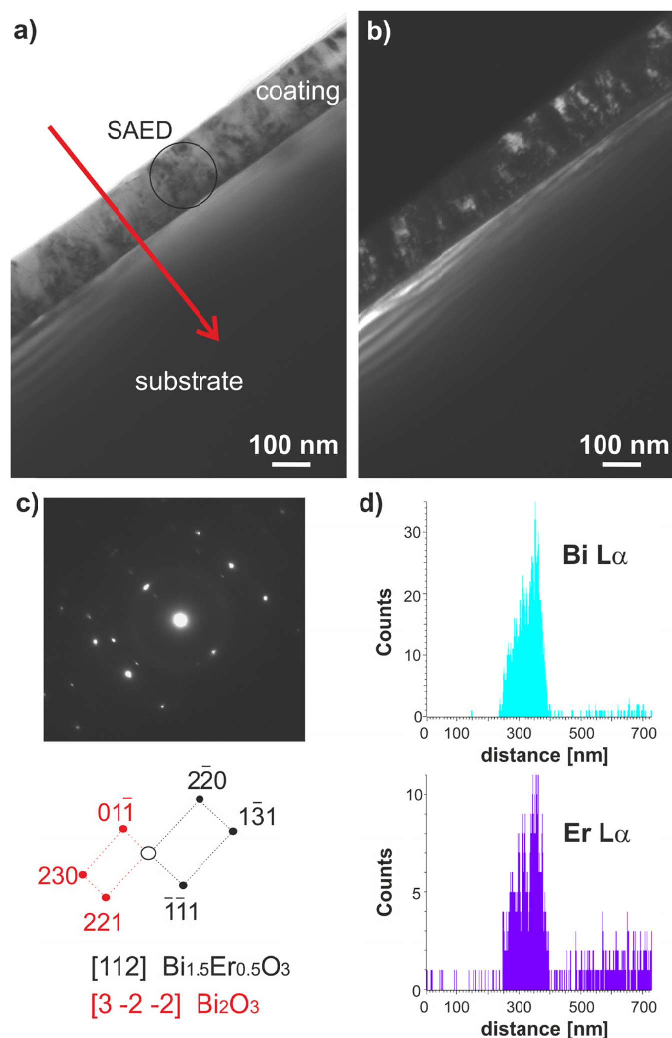

Fig. 7. Bright field TEM image of the $Bi_{1.5}Er_{0.5}O_3$ thin film deposited onto the sapphire substrate at T_{sub} of 600°C, film thickness 150 nm (a), dark field TEM image taken from the (–1-11) diffraction spot of the $Bi_{1.5}Er_{0.5}O_3$ (b), SAED pattern and its identification (c), STEM-EDS line analysis of Bi and Er distribution in the coating along the line marked in Fig. 7a. (d); FIB lamella

150 nm, the diameter of these columns was 25-75 nm, while their length was usually comparable with the film thickness. This was because the columns grow from the substrate to the film surface. Moreover, in thin films up to approx. 250 nm thick, any blisters, porosities or delamination were not observed. They are compact, with high density and low roughness. However, as shown earlier (Fig. 2, 4), in films with the thickness above 2 μm, there were numerous empty spaces between the columns. This phenomenon was observed in all films which thickness was on the order of 1.5-2.5 μm.

The selected area electron diffraction (SAED) pattern revealed the presence of the dominant $Bi_{1.5}Er_{0.5}O_3$ (fcc) phase in the film (Fig. 7c), i.e. the phase that was also identified by X-ray diffraction analysis and which corresponds to the structure of the high temperature phase δ-Bi_2O_3 in pure bismuth oxide. In addition, weak diffraction spots occurred in the pattern that could be identified as Bi_2O_3 with a tetragonal crystal structure. This phase however, was not detected by XRD analysis, likely due to its relatively low volume fraction. The results of the STEM-EDS line analysis (Fig. 7d) confirmed clearly the presence of Bi and Er in the thin film.

The surface topography measurements were performed using atomic force microscopy (AFM) on the surface of thin films deposited on Al_2O_3 substrate (0001) and containing a different amount of erbium (Fig. 8). The islands observed in the AFM images are likely the tops of the thin film columns. Their diameter is approximately 30-100 nm. Columns observed in the TEM images have a similar diameter. The surface roughness parameter RMS (Root Mean Square) for thin films containing different dopant content varies from 2.98 nm to 4.66 nm, however, no significant dependence of surface roughness on the erbium content was observed.

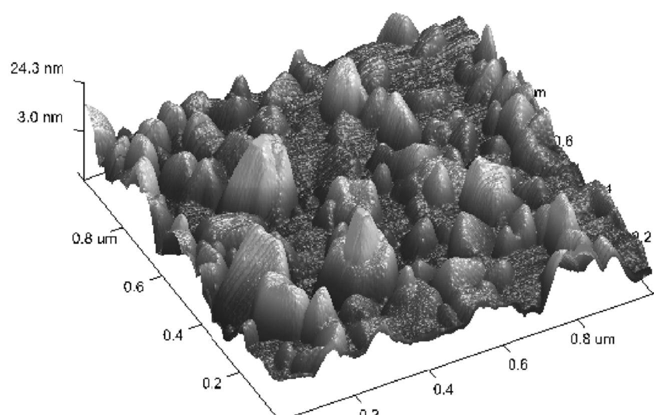

a) 20 mol % Er_2O_3;

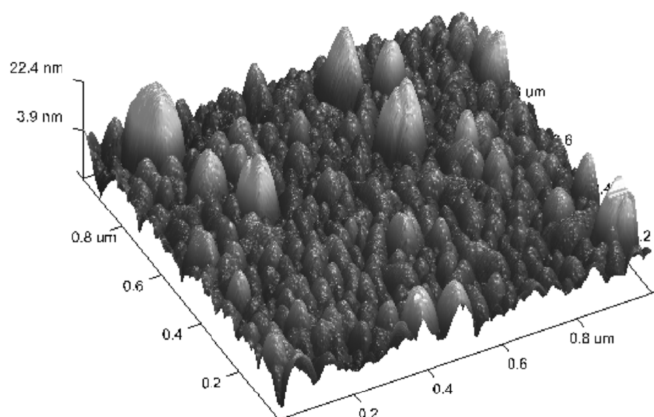

b) 25 mol % Er_2O_3

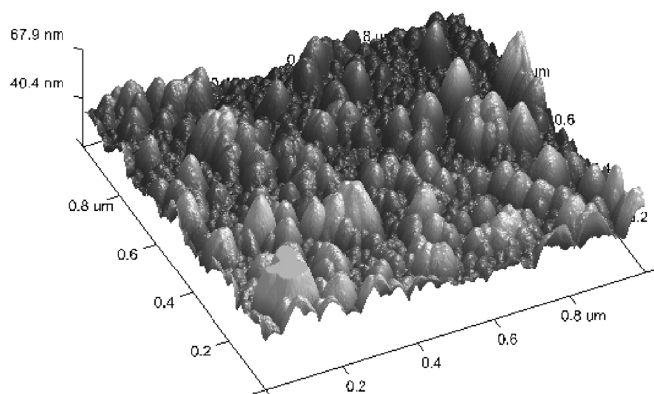

c) 30 mol % Er_2O_3

Fig. 8. AFM surface topography images of $Bi_{1.5}Er_{0.5}O_3$ thin films deposited onto the sapphire substrate at T_{sub} of 600°C; 20 mol % Er_2O_3, roughness parameter RMS = 4.66 nm (a), 25 mol % Er_2O_3, roughness parameter RMS = 2.98 nm (b), 30 mol % Er_2O_3, roughness parameter RMS = 4.17 nm (c)

4. Conclusions

The PLD processing of erbium stabilized bismuth oxide thin films deposition on c-sapphire (0001) substrate was developed. The produced thin films contained mainly the $Bi_{1.5}Er_{0.5}O_3$ phase that was stable at room temperature, which was the aim of the work. This phase crystallizes as face centered cubic system, (fluorite type, Fm-3m space group), which corresponds to the high temperature δ phase in pure bismuth oxide, with high ionic conductivity. All bismuth oxide thin films, regardless of the amount of Er dopant, have a columnar structure. In bismuth oxide films stabilized with erbia, up to 250 nm thick, the columns have a diameter at the base from 25 to 75 nm. In the case of films having low thickness, (in the range of 150-250 nm), the material of thin films is compact. The columns densely and tightly fill the entire volume of the films. While the film thickness increases, their porosity increases too, and discontinuities between the columns appear.

The rate of growth of thin films with the PLD parameters used is about 0.05 nm/laser pulse.

Acknowledgements

Financial support from National Science Centre under Grant Number 2011/03/B/ST8/05152 is highly appreciated.

REFERENCES

[1] S. Sanna, V. Esposito, C. Mogens, P. Nini, APL Mater. **4**, 121101_1-121101_5 (2016).
[2] T. Liu, Y. Zhao, L. Gao, J. Ni, Sci. Rep. **5**, 9307-9314 (2015).
[3] Y. Li, M.A. Trujillo, E. Fu, B. Patterson, L. Fei, Y. Xu, S. Deng, S. Smirnov, H. Luo, Bismuth oxide: a new lithium-ion battery anode, J. Mater. Chem. A. **1**, 12123-12127 (2013).
[4] E.D. Wachsman, K.T. Lee, Science, **334**, 935-939 (2011).
[5] D. Shan, J. Zhang, H.-G. Xue, Y.-C. Zhang, S. Cosnier, S.-N. Ding, Biosens. Bioelectron. **24**, 3671-3676(2009).
[6] Y. Qiu, D. Liu, J. Yang, S. Yang, Adv. Mater. **18**, 2604-2608 (2006).
[7] N. Arora, G. Deo, I.E. Wachs, A.M. Hirt, J. Catal. **159**, 1-13 (1996).
[8] W.K. Sakamoto, D.H.F. Kanda, C.L. Carvahlo, J. Mater. Sci. **19**, 603-605 (2000).
[9] V. Fruth, M. Popa, D. Berger, R. Ramer, M. Gartner, A. Ciulei, M. Zaharescu, J. Eur. Ceram. Soc. **25**, 2171-2174 (2005).
[10] K. Shimanoe, M. Suetsugu, N. Miura, N. Yamazoe, Solid State Ion. **113-115**, 415-419 (1998).
[11] M. Mehring, Coord. Chem. Rev. **251**, 974-1006 (2007).
[12] N. Cornei, N. Tancet, F. Abraham, O. Mentre, Inorg. Chem. **45**, 4886-4888 (2006).
[13] A.C. Jones, P.L. Chalker, J. Phys. D **36**, R80-R95 (2003).
[14] N.M. Sammes, G.A. Tompsett, H. Nafe, F. Aldinger, J. Eur. Ceram. Soc. **19**, 1801-1826 (1999).
[15] P. Shuk, H.-D. Wiemhofer, U. Guth, W. Gopel, M. Greenblatt, Solid State Ion. **89**, 179-196 (1996).
[16] S. Sanna, V. Esposito, C. Graves, J. Hjelm, J.W. Andreasen, N. Pryds, Solid State Ion. **266**, 13-18 (2014).
[17] V. Fruth, A. Ianculescu, D. Berger, S. Preda, G. Voicu, E. Tenea, M. Popa, J. Eur. Ceram. Soc. **26**, 3011-3016 (2006).
[18] C.D. Ling, R.L. Withers, S. Schmid, J.G. Thompson, J. Solid State Chem. **137**, 42-61 (1998).
[19] T. Takahashi, H. Iwahara, Mater. Res. Bull. **13**, 1447-1453 (1978).
[20] S.F. Radev, V.I. Simonov, Y.F. Cargin, Acta Crystallogr. B. **48**, 604-609 (1992).
[21] T.P. Gujar, V.R. Shinde, C.D. Lokhande, R.S. Mane, S.-H. Han, App. Surf. Sci. **252**, 2747-2751 (2006).
[22] O. Riko-Fuentes, E. Sanchez-Aguilera, C. Velasquez, R. Ortega-Alvarado, J.C. Alonso, A. Ortiz, Thin Solid Films **478**, 96-102 (2005).
[23] L. Leontie, M. Caraman, M. Alexe, C. Harnagea, Surface Science, **507**, 480-485 (2002).
[24] E.W. Bohannan, C.C. Jaynes, M.G. Shumsky, J.K. Barton, J.A. Switzer, Solid State Ion. **131**, 97-107 (2000).
[25] A.Z. Adamyan, Z.N. Adamyan, V.M. Aroutiounian, Sens. Actuator B-Chem. **93**, 416-421 (2003).
[26] M. Vehkamaki, T. Hatanpaa, M. Ritala, M. Leskela, J. Mater. Chem. **14**, 3191-3197 (2004).
[27] L. Leonite, M. Caraman, A. Visinoiu, G.I. Rusu, Thin Solid Films, **473**, 230-235 (2005).
[28] M. Le Thang, M. Kovanda, V. Myslik, M. Vrnata, I. Van Driessche, S. Hoste, Thin Solid Films, **497**, 284-291 (2006).
[29] J.-W. Sun, L.-S. Kang, J.-S. Kim, M.-R. Joung, S. Nahm, T.-G. Seong, et al., Acta Materialia **59**, 5434-5439 (2011).
[30] S. Kac, L. Cieniek: Inzynieria Materialowa **6**, 568- 571 (2008).
[31] S. Kac, T. Moskalewicz; Inzynieria Materialowa **4**, 295-298 (2013).
[32] S. Kac, L. Cieniek, T. Moskalewicz, Inzynieria Materialowa **36**, 479-483 (2015).
[33] G. Szwachta, S. Kac, T. Moskalewicz, Surf. Coat. Techn. **30**, 474-481 (2016).
[34] N. Jiang, E. D. Wachsman, J. Am. Ceram. Soc. **82**, 3057-3064 (1999).
[35] S. Sanna, V. Esposito, J.W. Andreasen, J. Hjelm, W. Zhang, T. Kasama, S.B. Simonsen, M. Christensen, S. Linderoth, N. Pryds, Nature Materials **14**, 500-504 (2015).
[36] M.J. Verkerk, K. Keizer, A.J. Burggraaf, J. Appl. Electrochem. **10**, 81-88 (1980).
[37] H. Kruidhof, K. Seshan, G.M.H. van de Velde, K.J. de Vries, A.J. Burggraaf, Mater. Res. Bull. **23**, 371-377 (1988).
[38] R.D. Shannon, Acta Crystallogr., Sect. A: Cryst. Phys. Diffr., Theor. Gen. Crystallogr. **32** (5) 751-67 (1976).
[39] S.J. Jeong, N.W. Kwak, P. Byeon, S.-Y. Chung, W.C. Jung, ACS Appl. Mater. Int. **10**, 6269-6275 (2018).